Soft Matter

One-dimensional collective migration of a proliferating cell monolayer

SCHOLARONE™
Manuscripts

Journal Name

One-dimensional collective migration of a proliferating cell monolayer

Pierre Recho[a,c], Jonas Ranft[b] and Philippe Marcq[c]

The importance of collective cellular migration during embryogenesis and tissue repair asks for a sound understanding of underlying principles and mechanisms. Here, we address recent *in vitro* experiments on cell monolayers which show that the advancement of the leading edge relies on cell proliferation and protrusive activity at the tissue margin. Within a simple viscoelastic mechanical model amenable to detailed analysis, we identify a key parameter responsible for tissue expansion, and we determine the dependence of the monolayer velocity as a function of measurable rheological parameters. Our results allow us to discuss the effects of pharmacological perturbations on the observed tissue dynamics.

1 Introduction

Recent experiments on the expansion dynamics of epithelial cell monolayers highlighted a propagative mode with an approximately constant velocity at the leading edge. They were performed with Madin-Darby canine kidney (MDCK) epithelial cells in a quasi-one-dimensional geometry, first on tracks of small width[1], then on a (cylindrical) fiber of small radius[2]. The presence of a free boundary gives rise to an inhomogeneous cell density along the tissue, increasing monotonically towards the rear of the cell layer. Conversely, the velocity is maximal at the leading edge and decreases monotonically with the distance from the front. Collective cell migration in the rear comes to a halt as cell density rises with time[3].

Studying epithelization over durations short compared to the typical cell cycle, some among us showed that a cell monolayer on a hard substrate may be described by an inviscid, incompressible fluid driven by active boundary forces[4]. A detailed comparison of model predictions with experimental measurements showed that during the epithelization of a disc-shaped empty domain, protrusive activity at the leading edge dominated force generation and external friction between monolayer and substrate dominated energy dissipation.

Motivated by the experiments mentioned above, we wish to extend these results to monolayer expansion assays whose duration is longer than a typical cell cycle. In addition to lamellipodial activity at the leading edge, cell proliferation, as well as inflow of cells from the reservoir, may drive collective migration. We take

into account variations of the cell density and use linear non-equilibrium thermodynamics to relate the equation of state of the tissue to the dependence of the proliferation rate on cell density. In doing so, we aim to provide a biophysical understanding of the tissue dynamics observed in experiments, which further allows to account for the effects of drug treatments that modify the velocity at the leading edge[1,2]. Our approach is complementary to earlier studies addressing mainly the kinetics of collective migration without reference to the tissue mechanical behaviour[5–7]. In the following, the cell monolayer will be loosely referred to as the "tissue" although it lacks some of the complexity of *in vivo* tissues, such as, *e.g.*, collagen secretion and organization.

This article is organized as follows. In Sec. 2, we introduce a one-dimensional mechanical description of the collective migration of a proliferating cell monolayer. The combination of forces generated by protrusions at the leading edge and by proliferation in the bulk leads to monolayer expansion at constant front velocity. We thus study in Sec. 3 the existence of traveling wave solutions and the dependence of the front velocity upon control parameters. The limit of vanishing viscosity, presented in Sec. 4, gives rise to an effective Fisher-Kolmogorov-like free-boundary problem which has a clear mechanical interpretation. In Sec. 5, we discuss how pharmacological perturbations may modify the response of the tissue. Finally, we summarize and discuss our results in Sec. 6.

2 Expansion of a proliferating cell monolayer

With highly cohesive cell monolayers in mind, we formulate a continuum description of collective migration. We describe the tissue at length scales large compared to the size of a single cell, and thus define the coarse-grained fields of the cell number den-

[a] *Mathematical Institute, University of Oxford, Oxford OX26GG, United Kingdom.*
[b] *Laboratoire de Physique Statistique, École Normale Supérieure, 24 rue Lhomond, F-75231 Paris Cedex 05, France*
[c] *Sorbonne Université, UPMC Univ Paris 06, Institut Curie, CNRS, UMR 168, Laboratoire Physco-Chimie Curie, Paris, France E-mail: philippe.marcq@curie.fr*
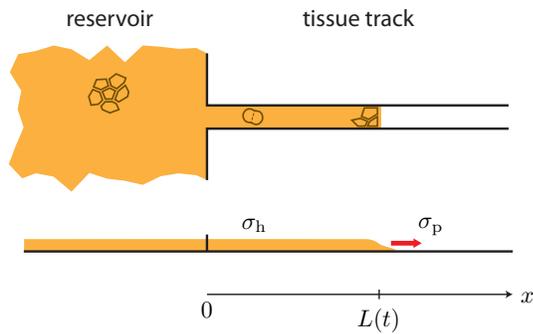
Fig. 1 Schematic representation of the one-dimensional expansion of a proliferating cell monolayer. (Top) A reservoir, which is occupied by a confluent cell monolayer, is connected to a smaller track to which the advancing cells are confined. Cells can undergo division and apoptosis, and cells at the leading edge exert pulling forces on the tissue due to lamellipodial activity. (Bottom) Side view of the upper sketch; σ_h denotes the homeostatic stress at which cell division and cell death balance, and σ_p denotes the protrusive stress exerted at the leading edge. (Online version in colour.)

sity $\rho(\vec{r},t)$, the velocity $v(\vec{r},t)$ and the stress $\sigma(\vec{r},t)$ as functions of the space coordinate $\vec{r}$ and time t. Sec. 2.1 recapitulates the conservation laws obeyed by the system. Sec.2.2 shows that the framework of linear non-equilibrium thermodynamics relates the cell density dependence of stress and proliferation rate. Sec. 2.3 gives the resulting evolution equations and boundary conditions in dimensionless form.

2.1 Conservation laws

In order to describe the migration of a cell monolayer along narrow tracks or along cylindrical fibers of small radii, we assume that the relevant fields vary little across the track width or the fiber circumference. This assumption implies the absence of long-range velocity correlations that are known to occur for track widths larger than $100\,\mu\mathrm{m}$[1], the order of magnitude of the velocity correlation length as measured in bulk.

Within a thin film approximation, we consider an effectively one-dimensional system along the migration axis: $\vec{r} = x\vec{e}_x$. At time t, the tissue covers the track, or the fiber, from a reservoir at $x = 0$ to the leading edge at $L(t)$, see Fig. 1 for a sketch. Importantly, cells belong to a monolayer everywhere, including in the reservoir, and there is no "permeation" of cells from superior layers as in the case of a cell monolayer spreading from an aggregate with weaker cell-cell adhesion[8]. Since the cell monolayers that we consider are easily supplied with nutrients from the third dimension, *i.e.*, from the culture medium at the apical side, growth is not limited by nutrient diffusion within the tissue. Because the extracellular fluid is not confined to the tissue layer, we can neglect interstitial flows that would otherwise give rise to additional mechanical constraints[9,10]. We furthermore do not consider here the effect of external chemotactic fields[11].

Cell conservation law. The cell number density obeys the mass balance equation, supplemented with a source term due to cell proliferation:

$$\partial_t \rho + \partial_x (\rho v) = k_\mathrm{d}(\rho)\,\rho \tag{1}$$

where k_d is the effective proliferation rate, combining cell divisions and cell deaths (delaminations), and depends on cell density, see below. This conservation law is associated with boundary conditions at the inlet, where the tissue is connected to the reservoir, and the free end of the tissue. In line with experiments, we impose zero flux boundary conditions:

$$v(0,t) = 0 \qquad \text{and} \tag{2}$$

$$v(L(t),t) = \dot{L}(t), \tag{3}$$

respectively. Throughout the text, $\dot{} = \mathrm{d}/\mathrm{d}t$ denotes the total derivative with respect to time. Eq. (2) assumes that cell proliferation in the reservoir and subsequent tissue inflow is negligible compared to proliferation in the tissue, as observed experimentally[3]. Eq. (3) provides a kinematic condition for the evolution of the leading edge. In principle, it could be modified by including a boundary growth term if necessary.

Proliferation rate. Consistent with observations[3,12], we consider that the proliferation rate depends on cell density and assume for simplicity a linear relation[13,14],

$$k_\mathrm{d}(\rho) = \frac{1}{\tau_\mathrm{d}} \frac{\rho_\mathrm{d} - \rho}{\rho_\mathrm{d}}, \tag{4}$$

where ρ_d is the tissue carrying capacity, in other words the reference cell density at which the net cell division rate vanishes. [See Appendix A for the more general case of arbitrary $k_\mathrm{d}(\rho)$.] The characteristic time scale τ_d may be estimated experimentally[12] for vanishing cell densities as $\tau_\mathrm{d} = k_\mathrm{d}(0)^{-1}$. Note that the coupling between density and proliferation is not *per se* mechanical but may be a combined effect of mechanical compression and density-dependent signaling between cells. One declared aim of this paper is to investigate the ramifications of such a coupling for migrating tissues.

Force balance. In this continuum framework, internal and external forces are respectively described by the stress field $\sigma(x,t)$ and the external force field $f^\mathrm{ext}(x,t)$. Force balance is expressed as

$$\partial_x \sigma = -f^\mathrm{ext}. \tag{5}$$

We assume that external forces are due to fluid friction between the tissue and the substrate[4]:

$$f^\mathrm{ext} = -\xi v. \tag{6}$$

For simplicity, we neglect active, bulk motility forces, as may be produced by, *e.g.*, cryptic lamellipodia within the monolayer[15]. At the free boundary $x = L(t)$ however, leading cells extend lamellipodia and exert active pulling forces on the rest of the tissue. Mechanically, we therefore treat boundary cells at the front as external agents applying a tensile traction σ_p on the monolayer, leading to the following condition on the stress[4]:

$$\sigma(L(t),t) = \sigma_p. \tag{7}$$

2.2 Linear non-equilibrium thermodynamics

In order to close the system of equations and to fully specify the tissue mechanics, one needs a constitutive equation to relate stresses to quantities like the cell density and the cell velocity field. It is generally assumed that an equation of state relates the isotropic tissue stress to the cell density, and that viscous stresses occur in the presence of velocity gradients, effectively leading to a Kelvin-Voigt viscoelastic rheology in one dimension.

Instead of postulating *ad hoc* such a relation, we use the framework of linear non-equilibrium thermodynamics [16] to specify the constitutive equation of the cell monolayer, see [17] for a similar derivation in the context of single cell migration. This approach has the advantage of being systematic in terms of the identified fluxes and forces once a free energy is specified, and to give a coherent picture of the dissipation caused by the system. More specifically, it allows us to identify an equation of state for the tissue stress that is thermodynamically consistent with the linear relation $k_d(\rho)$ chosen above. To express the dissipation rate in the material, we follow the classical Coleman-Noll method [18–20] (see also [21] for a general treatment in the context of volumetric growth).

However, as one may argue that tissues are too far from (thermodynamic) equilibrium for linear non-equilibrium thermodynamics to hold and that the assumption of the existence of a well-defined free-energy density that depends on a few variables of the system may not be justified, we refer the reader to Appendix A for a more general treatment.

In the presence of distributed (bulk) friction forces $f^{\text{ext}} = -\xi v$ and of (boundary) traction forces σ_p due to lamellipodial protrusions at the leading edge, the power Π of the *external* forces to which the monolayer is subjected reads

$$\Pi = -\int_0^L \xi v^2 \, dx + \sigma_p \dot{L}$$

$$= \int_0^L (-\xi v^2 + \partial_x(\sigma v)) \, dx.$$

By taking into account the force balance equation (5), Π can also be expressed as the power of the *internal* forces

$$\Pi = \int_0^L \sigma \partial_x v \, dx.$$

The total free energy of the cell monolayer reads

$$F = \int_0^L \rho f(\rho) \, dx,$$

where $f(\rho)$ is the specific free energy, which we assume to be dependent only on the cell density ρ since temperature is constant in the tissue and heat fluxes can thus be neglected. A theory describing a more general growth process is currently under investigation and will be published elsewhere. Using Reynolds' theorem, the rate of change of the free energy reads

$$\dot{F} = \int_0^L k_d \rho f \, dx + \int_0^L \rho^2 \frac{df}{d\rho}(k_d - \partial_x v) \, dx.$$

In this isothermal system the power of external forces and the free

energy rate must satisfy a dissipation principle

$$\Sigma = \Pi - \dot{F} \geq 0.$$

We express Σ as a bilinear form

$$\Sigma = \int_0^L (\sigma + p)\partial_x v \, dx + \int_0^L (-\rho\mu)k_d \, dx.$$

where $p = \rho^2 \frac{df}{d\rho}$ is the thermodynamic pressure and $\mu = f + \frac{p}{\rho}$ is the thermodynamic chemical potential [22] whose role in three dimensional elasticity is played by the corresponding component of the energy momentum Eshelby tensor [21]. The two terms under integrals can be interpreted as products of the thermodynamic forces $\sigma + p$, $-\rho\mu$ with the respective conjugate thermodynamic fluxes $\partial_x v$, k_d.

Constitutive equations are obtained by expressing thermodynamic forces as a linear combination of thermodynamic forces through Onsager type relations. For simplicity, we neglect the cross-terms, and obtain

$$\sigma + p = l_{11} \partial_x v \tag{8a}$$

$$-\rho\mu = l_{22} k_d. \tag{8b}$$

Here the different tensorial nature of the fluxes/forces is not an issue because of the 1D Ansatz. Both diagonal kinetic coefficients l_{11} and l_{22} are positive and we shall from now on denote $\eta = l_{11}$ the viscosity. We are left with the conventional relation (8a) for a viscous, one-component, compressible fluid at a constant temperature [22]

$$\sigma = -p + \eta \partial_x v$$

Identity (8b) relates the proliferation rate to its naturally associated generalized force, the chemical potential [23,24]. Interestingly, the only choice of free energy consistent with the form of k_d assumed in Eq. (4) leaving ρ unconstrained, is then

$$f(\rho) = \frac{l_{22}}{\rho \tau_d} \left(\log\left(\frac{\rho_e}{\rho}\right) + \frac{\rho}{\rho_d} - 1 \right),$$

where we have imposed the condition $p(\rho_e) = 0$, introducing an *elastic* reference density ρ_e. Importantly, $\rho_d \neq \rho_e$: the carrying capacity does not need to be equal to the elastic reference density. This leads to an expression of the stress thermodynamically consistent with (4),

$$\sigma = -E \log\left(\frac{\rho}{\rho_e}\right) + \eta \frac{\partial v}{\partial x}, \tag{9}$$

where we identify the prefactor $E = l_{22}/\tau_d$ as the elastic modulus of the tissue.

The monotonically decreasing function $s_e(\rho) = -\log(\rho/\rho_e)$ characterizes the dependence of (elastic) stress upon density allowing to consider large deformations of the material. It is identical to the true strain, and infinitely penalizes both infinite dilution ($\rho = 0$) and the formation of singularities ($\rho = \infty$). While the same form was postulated for convenient technical reasons in [25–27] to describe wound healing and cell colony expansion, we show here that it is consistent with a proliferation rate linear in the density

as assumed in Eq. (4).

2.3   The model

We now formulate the problem of cell monolayer expansion, assuming for simplicity that the material parameters τ_d, ρ_d, η, ξ, σ_p, ρ_e and E are constant.

We use τ_d, $\sqrt{\frac{E\tau_d}{\xi}}$, ρ_d and E as units of time, length, density and stress respectively, and the reduced stress field

$$s = \frac{\sigma - \sigma_p}{E}.$$

The velocity field can be expressed as a stress gradient using (5) and (6). Combining (1) with (4) as well as (5) with (9) we obtain the dimensionless evolution equations

$$\frac{\partial \rho}{\partial t} + \frac{\partial}{\partial x}\left(\rho \frac{\partial}{\partial x} s\right) = (1-\rho)\rho \tag{10}$$

$$\tilde{\eta} \frac{\partial^2 s}{\partial x^2} - s = \log \rho + \alpha \tag{11}$$

with boundary conditions

$$\partial_x s(0,t) = 0 \tag{12a}$$

$$\partial_x s(L(t),t) = \dot{L}(t) \tag{12b}$$

$$s(L(t),t) = 0. \tag{12c}$$

The dynamics of the free front depends only on *two* dimensionless parameters: an active driving

$$\alpha = \frac{\sigma_p}{E} + \log \frac{\rho_d}{\rho_e} \tag{13}$$

and a dimensionless viscous coefficient

$$\tilde{\eta} = \frac{\eta}{E\,\tau_d}. \tag{14}$$

In order to discuss the physical origin of the active driving characterized by the parameter α, it is instructive to consider the stationary, homogeneous solution of Eqs. (10-12), given by $\rho = 1$, $s = -\alpha$, $v = 0$, and vanishing front velocity $\dot{L}(t) = 0$. Returning to dimensionful quantities, stationarity of the tissue requires that cell division and apoptosis balance on average, which according to Eq. (4) occurs for $\rho = \rho_d$. This state of tissue homeostasis implies that bulk stresses are everywhere constant and equal to a homeostatic stress

$$\sigma_h = -E\log \frac{\rho_d}{\rho_e}$$

which needs to be balanced at the tissue margin and thus requires $\sigma_p = \sigma_h$. Given the definition (13), the stationary solution is only possible for zero active driving $\alpha = 0$.

The active driving α can thus be expressed as the difference between the protrusive stress exerted at the free edge and the homeostatic stress, normalized by the tissue elastic modulus,

$$\alpha = \frac{\sigma_p - \sigma_h}{E}.$$

When $\alpha \neq 0$, the homeostatic state cannot be sustained, and $\rho = \rho(x) \neq \rho_d$. In this case, net cell division ($k_d > 0$ for $\alpha > 0$) or death ($k_d < 0$ for $\alpha < 0$) at the front give rise to tissue expansion or contraction, respectively, the dynamics of which is prescribed by Eqs. (10-11), see Sec. 3.1.

A finite homeostatic stress $\sigma_h \neq 0$ implies a mismatch between the carrying capacity ρ_d and the elastic reference density ρ_e, which is often considered in elastic growth theories as a source of growth-induced stress (see e.g. [28,29]). The ratio between the applied stress at the free boundary to the elastic modulus of the tissue, σ_p/E, which quantifies the strength of the pulling forces exerted by the cells at the leading edge, can also be related to a spreading coefficient within the context of wetting dynamics [8,30].

If $\sigma_p \gg E$, the tissue may no longer be able to accommodate large deformations and will eventually rupture under tensile stress [31], a phenomenon inconsistent with the present formulation which assumes continuity of the tissue. Conversely, if $-\sigma_p \gg E$, a buckling instability may occur: this eventuality is also beyond the scope of the present quasi-1D approach. Recent work [31,32] suggests values for σ_h as well as for E of the order of a few kPa. We therefore expect the active driving $|\alpha|$ to be at most of order 1.

Before turning to the analysis, let us discuss the various scales involved in this problem. For lack of measurements performed in the one-dimensional case, we rely on data from two-dimensional cell monolayers [4,12,31] as well as three-dimensional cellular spheroids [33,34]. The dependence of cell cycle duration upon cell number density has been measured in [12], yielding a time scale $\tau_d \approx 10\,\text{h} \approx 10^4\,\text{s}$. Using $E \approx 10^3\,\text{Pa}$ [31] and $\xi \approx 10^{16}\,\text{Pa}\,\text{m}^{-2}$ s [4], we deduce a length scale of the order of $\sqrt{E\tau_d/\xi} \approx 30\,\mu\text{m}$, and a velocity scale $U = \sqrt{E/(\xi\,\tau_d)} \approx 10\,\mu\text{m}\,\text{h}^{-1}$, similar to typical cell migration velocities [1–3].

In agreement with the typical viscosity of cell aggregates [33,34], the viscosity of a MDCK cell monolayer has been measured in [31]: from $\eta \approx 10^5\,\text{Pa}\,\text{s}$, we find $\tilde{\eta} \approx 10^{-2}$. The associated viscous stresses can be estimated as follows. The velocity gradient in the tissue necessarily extends over several cells, and we estimate the order of magnitude of the strain rate as $\partial_x v \approx v_{typ}/100\,\mu\text{m} \approx 10^{-1}\,\text{h}^{-1}$ using the typical migration velocities mentioned above. Given a strain of order $\partial_x u \approx 10^{-1}$ and with $E \approx 10^3\,\text{Pa}$ [31], $\eta \approx 10^5\,\text{Pa}\,\text{s}$ [33,34], one finds that $\eta\partial_x v/E\partial_x u \approx 2\,10^{-2}$. One can *a priori* expect viscous stresses to be negligible in the experiments. Note that most of the numerical values pertain to the epithelial MDCK cell line.

3   Traveling waves

In this section, we first study numerically the system (10-12), successively describing the transient dynamics (Sec. 3.1) and the propagating front (Sec. 3.2) that follows in the asymptotic regime when the active driving is extensile. We then derive analytically an exact traveling wave solution in the limit of $\alpha \to \infty$ (Sec. 3.3). The asymptotic front velocity is defined as $V = \lim_{t\to\infty} \dot{L}(t)$.

(a)

(b)
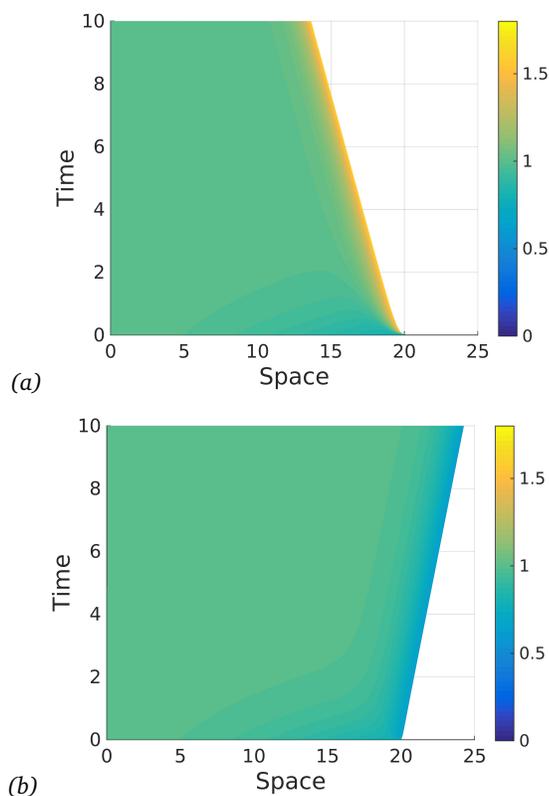
Fig. 2 Tissue contraction and expansion. Kymographs of the dimensionless cell density field $\rho(x,t)$ (density values given by the colourbar) showing *(a)* contraction, $\alpha = -0.5$ and *(b)* expansion, $\alpha = 0.5$. In both cases, $\tilde{\eta} = 10^{-2}$ and the initial condition for the cell density field is $\rho^0(x) = \exp\left\{-(x/(2L_0))^2\right\}$, $x \in [0, L_0]$, $L_0 = 20$. (Online version in colour.)

3.1 Transients

Numerical simulations of Eqs. (10-11) supplemented with boundary conditions (12) are performed thanks to the numerical scheme described in Appendix B. Given the initial profile for the density field $\rho(x, t = 0) = \rho^0(x)$, $x \in [0, L_0]$, the initial profile $\sigma^0(x)$ for the stress field is obtained by solving (11), the spatial derivative of which gives the initial velocity field $v^0 = d\sigma^0/dx$. We checked that the asymptotic behavior does not depend on the choice of $\rho^0(x)$. As explained above, we qualitatively expect the monolayer to contract when $\alpha < 0$ and to expand when $\alpha > 0$, regardless of the value of the viscosity.

Contraction. Our simulations confirm that $\alpha < 0$ leads to tissue contraction, see Fig. 2(a) for a typical kymograph. Consistent with the qualitative argument presented in Sec. 2.3, one observes $\rho(x) \geq \rho_d$ close to the leading edge, implying a negative net cell division rate and progressive suppression of the tissue layer. After a short transient, contraction is approximately linear with time: a propagative wave forms whose constant velocity V is a function of the active driving α and the viscosity $\tilde{\eta}$, see Fig. 3. One can define a characteristic time until collapse t_c as being the time when $L(t_c) = L_c \ll 1$. For large initial tissue sizes, $L(t = 0) = L_0 \gg 1$, we find $t_c \simeq L_0/V$. Interestingly, recent numerical and experimental

work[32] suggests that, in a number of cases, tissue homeostasis is a state of mechanical tension, characterized by a positive homeostatic stress $\sigma_h > 0$. For zero protrusive stress $\sigma_p = 0$, Eq. (13) then gives $\alpha < 0$: full inhibition of the protrusive activity of leader cells may result in tissue contraction.

Expansion. In line with the experiments that motivate this work, we focus on the opposite case $\alpha > 0$ in the remainder of this article. After a transient, whose duration increases with $\tilde{\eta}$ and decreases with α, the tissue dynamics converges towards a spreading regime with a propagating front with constant velocity V, see Fig. 2(b), in agreement with observations[1,2]. Here $\rho(x) \leq \rho_d$: cell density decreases, whereas velocity increases with x, velocity being maximal at the leading edge.

3.2 A propagating front

In the experimentally relevant case of monolayer expansion $\alpha > 0$, we next ask how the asymptotic front velocity V depends on the parameters α and $\tilde{\eta}$. From (10-12), it satisfies the following problem on the half-axis $z = x - Vt \in]-\infty, 0]$,

$$-V\rho' + (s'\rho)' = \rho(1-\rho),$$

$$\tilde{\eta}s'' - s = \log\rho + \alpha,$$

$$\rho(-\infty) = 1, \qquad s(0) = 0, \tag{15}$$

$$s'(0) = V, \quad s'(-\infty) = 0,$$

where $\rho(z) = \rho(x,t)$, $s(z) = s(x,t)$ and $z = 0$ is the position of the free front. A prime $' = \frac{d}{dz}$ denotes the derivative with respect to the reduced variable z.

To numerically compute $V(\alpha, \tilde{\eta})$, we choose to operate by continuation from the known value $V = 0$ at $\alpha = 0$ using AUTO[35]. From this value, the software follows the solution of the nonlinear system (15) when α varies (negatively or positively) using a Newton algorithm. We checked that the velocities thus obtained are identical to those attained in the asymptotic regime using direct numerical simulation. In Fig. 3, we plot $V(\alpha, \tilde{\eta})$ as a function of α for several values of $\tilde{\eta}$. Using the velocity scale $U = \sqrt{E/(\xi\tau_d)} \approx 10\,\mu\mathrm{m\,h}^{-1}$ (see Sec. 2.3), the experimentally observed front velocities are of $\mathcal{O}(1)$ [1,3] and thus suggest that $\alpha \approx 1 - 2$, consistent with our upper bound estimate $\alpha \lesssim \mathcal{O}(1)$.

We observe that the front velocity increases linearly with α for $|\alpha| \ll 1$, and eventually saturates for $\alpha \to \infty$ to a value that *increases* with $\tilde{\eta}$. The counterintuitive behaviour of V with the viscosity can be understood qualitatively as follows. By integration of (15), the front velocity can be expressed as a function of cell density only,

$$V = \int_{-\infty}^{0} \rho(z)(1 - \rho(z))\,dz.$$

Thus, cell proliferation contributes to propulsion only in the interfacial layer between the (homeostatic) state $\rho = 1$ and the tissue margin density $\rho(z = 0)$. The speed of the front depends both on the density range given by $1 - \rho(0)$ and on the width λ of the interfacial layer. For $\alpha \to \infty$, the former is bounded by 1, whereas λ grows with $\tilde{\eta}$ since viscous dissipation penalizes large gradi-
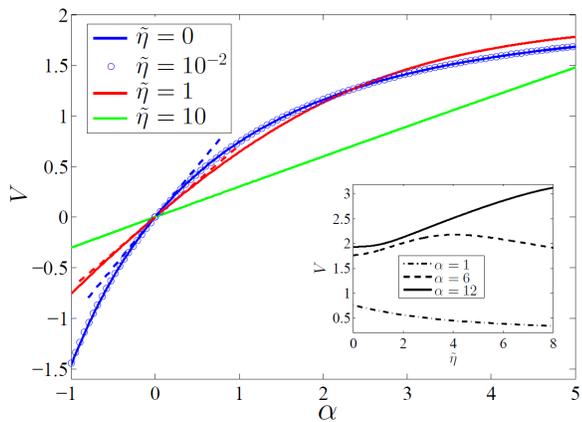
Fig. 3 Front velocity. The dimensionless velocity $V(\alpha, \tilde{\eta})$ is plotted as a function of the control parameter α, for several values of the dimensionless viscosity $\tilde{\eta}$. Values obtained for $\tilde{\eta} = 10^{-2}$ (blue circles) are indistinguishable from those obtained in the inviscid limit $\tilde{\eta} = 0$ (solid blue line). The dashed lines represent the linear approximation close to $(\alpha = 0, V = 0)$: $V = \alpha/\sqrt{1+\tilde{\eta}}$, see Sec. 3.3. Inset: $V(\alpha, \tilde{\eta})$ *vs.* $\tilde{\eta}$ for fixed values of α. For small enough α (dot-dashed curve) the velocity decreases with $\tilde{\eta}$ as captured by linear analysis (see Sec. 3.3). For larger values of α, note the non-monotonic viscosity-dependence of the front velocity (dashed curve) which first increases with $\tilde{\eta}$ and then decreases after a critical value of $\tilde{\eta}$ is reached. This critical value increases with α and ultimately, when $\alpha \to \infty$, the front velocity becomes a monotonically increasing funtion of $\tilde{\eta}$. (Online version in colour.)
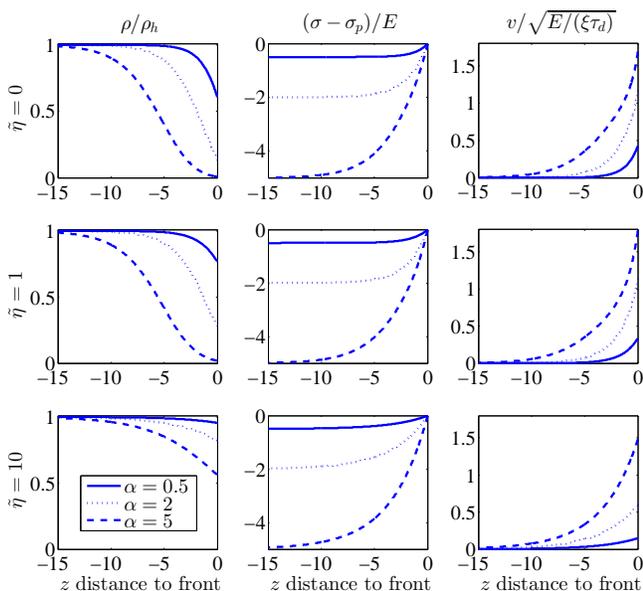
Fig. 4 Typical steady-state profiles of density, stress and velocity along the monolayer. (Online version in colour.)

ents. As a consequence, in this limit, the front moves faster for a larger viscosity (see Fig. 3 inset, full line). This situation is re-mindful of the "pushed" fronts observed in the propagation of an interface between two proliferating cell populations, where pro-liferation in the bulk occurs over a lengthscale that grows with

tissue viscosity, propelling the interface forward[36]. For $|\alpha| \ll 1$, a perturbative calculation shows that the velocity grows with α, and decreases with $\tilde{\eta}$ as $V = \alpha/\sqrt{1+\tilde{\eta}}$ (see Sec. 3.3). In this limit of small driving, the effect of $\tilde{\eta}$ is two-fold: viscous dissipa-tion both reduces $1 - \rho(0)$ and decreases the slope of the interface region, the joint effect of which is a decrease in the front velocity (Fig. 3 inset, dotted-dashed line). In between these two limits of large and small driving, an increase of $\tilde{\eta}$ may either increase or decrease the velocity depending on the values of both $\tilde{\eta}$ and α (Fig. 3 inset, dashed line).

In Fig. 4, we represent the steady-state profiles obtained by AUTO. Density, stress and velocity profiles connect the home-ostatic state $\rho = 1$, $s = -\alpha$, $v = 0$ in the bulk to the leading edge state $\rho = \rho(0)$, $s = 0$, $v = V$ at $z = 0$. For all parame-ter values, the asymptotic density profiles decrease monotoni-cally, whereas the velocity and stress profiles increase monoton-ically along the monolayer, in agreement with experimental ob-servations. Whether the tissue is under tension ($\sigma > 0$) or un-der compression (negative tension, $\sigma < 0$) does not depend on the sign of α but on the signs of both σ_h and σ_p. In general, $\min(\sigma_h, \sigma_p) \le \sigma \le \max(\sigma_h, \sigma_p)$, and while s is always negative, the tissue can switch from a compressive to a tensile state at some bulk point (or even be tensile everywhere) due to the action of leader cells.

We checked numerically that the monotonic profiles of the cell density, velocity and stress fields found asymptotically are stable to perturbations by an additive noise of small amplitude. Explain-ing the propagation of mechanical waves during two-dimensional tissue expansion[37] will therefore require additional ingredients, among which contractility-dependent bulk motility forces are an obvious candidate.

3.3 The small driving limit

For $\alpha \ll 1$, the velocity of the expanding tissue can be explicitly found as a function of α and $\tilde{\eta}$. Performing a Taylor expansion around the stationary state $\alpha = 0$, $s = 0$, $\rho = 1$, and $V = 0$, we have

$$s = 0 + \varepsilon \overset{1}{s} + o(\varepsilon), \qquad\qquad \rho = 1 + \varepsilon \overset{1}{\rho} + o(\varepsilon),$$

$$V = 0 + \varepsilon \overset{1}{V} + o(\varepsilon), \qquad\qquad \alpha = 0 + \varepsilon \overset{1}{\alpha} + o(\varepsilon),$$

where ε is a small, positive parameter $0 < \varepsilon \ll 1$, and $\overset{1}{q}$ denotes the first-order perturbation of quantity q. Eqs. (15) then become at first order

$$\overset{1}{s}'' = -\overset{1}{\rho} \qquad \text{and} \qquad \tilde{\eta}\overset{1}{s}'' - \overset{1}{s} = \overset{1}{\rho} + \overset{1}{\alpha}$$

with boundary conditions

$$\overset{1}{\rho}(-\infty) = \overset{1}{s}'(0) - \overset{1}{V} = \overset{1}{s}'(-\infty) = \overset{1}{s}(0) = 0.$$

Combining the first and second equation we obtain the second order differential equation

$$(\tilde{\eta}+1)\overset{1}{s}'' - \overset{1}{s} = \overset{1}{\alpha}$$

for the reduced stress field s to first order. Using boundary conditions on $\overset{1}{s}$ we obtain

$$\overset{1}{s} = \overset{1}{\alpha}\left(e^{\frac{z}{\sqrt{1+\tilde{\eta}}}} - 1\right) \quad \text{and} \quad \overset{1}{\rho} = -\overset{1}{\alpha}\frac{e^{\frac{z}{\sqrt{1+\tilde{\eta}}}}}{1+\tilde{\eta}}.$$

Spatial variations of velocity field, the stress field and the cell number density decay away from the front over a characteristic length

$$\Delta z = \sqrt{1+\tilde{\eta}}.$$

Since we expect $\tilde{\eta} \simeq 10^{-2}$, the size of this boundary layer is given by the unit of length, of the order of $\sqrt{E\tau_{\mathrm{d}}/\xi} \approx 30\,\mu\mathrm{m}$.

Of the two remaining boundary conditions, one is automatically satisfied while the last one provides the velocity,

$$V = \frac{\alpha}{\sqrt{1+\tilde{\eta}}}. \tag{16}$$

This expansion for $\alpha \ll 1$ can be made at all orders following the same procedure, defining an alternative way to analytically construct $V(\alpha, \tilde{\eta})$. We note that the linear approximation becomes accurate over a wider range of α as $\tilde{\eta}$ increases, see Fig. 3.

4　The inviscid limit

In this section, we consider the inviscid limit of (10-11) which corresponds to $\tilde{\eta} \to 0$ and is more amenable to analysis. This limit can be viewed as the limit where the effective viscosity due to cell division $E\tau_{\mathrm{d}}$ dominates the bulk hydrodynamic viscosity of the tissue, see Eq. (14). Plugging $s = -\log\rho - \alpha$ (see (11)) into (10) we obtain the following parabolic reaction-diffusion equation for the cell density field ρ,

$$\partial_t\rho = \partial_{xx}\rho + \rho(1-\rho), \tag{17}$$

using dimensionless quantities. When defined over the real axis, and for initial conditions decaying faster than exponentially, the Fisher-Kolmogorov equation (17) admits a traveling wave solution between the fixed points $\lim_{x\to-\infty}\rho = 1$ and $\lim_{x\to+\infty}\rho = 0$ with a velocity $V_{\mathrm{FK}} = 2$ [5,38,39]. This equation is a classical model of collective cell migration into empty space, originally introduced to describe the kinematics of wound healing assays [40,41] by combining the effects of cell diffusion and cell proliferation, yet without reference to mechanical aspects. Based on measurements of the front velocity and of the cell density profile, good agreement has been found with predictions of the Fisher-Kolmogorov equations for a variety of wound healing assays [6,7,42–46]. However, the smooth spatial variation of Fisher-Kolmogorov traveling waves is often hard to reconcile with the steepness of the cell density profile observed close to the leading edge [46]. This point has led to the study of a sharp-front Fisher-Kolmogorov equation, where the diffusion coefficient is a linear function of the cell density and vanishes when $\rho = 0$ [6,44,47].

Here, cell monolayer expansion corresponds to the associated free boundary problem posed on $x \in [0, L(t)]$ with the boundary conditions

$$\partial_x\rho(0,t) = 0, \tag{18a}$$

$$\rho(L(t),t) = e^{-\alpha}, \tag{18b}$$

$$\partial_x\rho(L(t),t) = -\dot{L}(t)e^{-\alpha}. \tag{18c}$$

Condition (18b) reflects the fact that the front is always sharp, with a finite density that follows from Eq. (7), and diffusion has a purely mechanical origin, distinct from the random motion of single cells within the tissue. Traveling wave solutions are known to exist for the problem (17-18) on the semi-axis $(-\infty, L(t)]$ [27] and the result of Fisher-Kolmogorov is recovered in the limit of strong active driving $\alpha \to \infty$.

Indeed, taking the limit in the Dirichlet boundary condition, Eq. (17) is supplemented with

$$\rho(L(t),t) = 0,$$

$$\partial_x\rho(L(t),t) = 0, \quad \text{and} \quad \partial_x\rho(0,t) = 0.$$

This problem belongs to the class of models studied in [48], where it is shown that regardless of initial conditions, linear expansion occurs. Further, Proposition 2.2 of [48] shows that the asymptotic velocity is

$$\dot{L}(t) \xrightarrow[t\to\infty]{} V_{\mathrm{FK}} = 2$$

in agreement with the Fisher-Kolmogorov result. We emphasize again that this limit of strong driving is unphysical.

As in the viscous case, the dependence of the front velocity V on the active driving α for the problem defined by Eqs. (17-18) is obtained numerically with the AUTO software [35], see Fig. 3. The asymptotic front velocity $V(\alpha)$ is a monotonically increasing function interpolating between $V(0) = 0$ and $V(\infty) = 2$. A simple approximation giving the correct velocities and slopes at both $\alpha = 0$ and $\alpha = \infty$ is the function $V_{\mathrm{approx}}(\alpha) = 2\left(1 - e^{-\alpha/2}\right)$. As seen in Fig. 3, the velocity curve $V(\alpha, \tilde{\eta})$ for a realistic viscosity $\tilde{\eta} = 10^{-2}$ is almost indistinguishable from $V(\alpha, 0)$, consistent with our above reasoning (Sec. 2.1) that viscous stresses are expected to be negligible.

In dimensional form, the front velocity is thus given by

$$\mathscr{V} = \sqrt{\frac{E}{\xi\tau_{\mathrm{d}}}}V\left(\frac{\sigma_{\mathrm{p}}}{E} + \log\frac{\rho_{\mathrm{d}}}{\rho_{\mathrm{e}}}\right) \tag{19}$$

where the function V is the dimensionless velocity computed numerically and drawn on Fig. 3.

We also show the asymptotic profiles for different values of α, see Fig. 4, top row. One can see that they display a boundary layer whose spatial extension Δx may be simply estimated in the following way,

$$V(\alpha) = -\left.\left(\frac{1}{\rho}\frac{\Delta\rho}{\Delta x}\right)\right|_L \simeq \frac{1-e^{-\alpha}}{e^{-\alpha}\Delta x},$$

or $\Delta x \simeq (e^{\alpha} - 1)/V(\alpha)$. When $0 < \alpha \ll 1$, in agreement with (3.3) we recover $\Delta x = 1$. When $\alpha \gg 1$, $\Delta x \to \infty$ since the transition between the values $\rho = 1$ and $\rho = 0$ may be located anywhere. Note

however that the moving interface associated with the Fisher-Kolmogorov solution, where this transition occurs, still has a finite width of $\mathscr{O}(1)$.

5 Possible effects of pharmacological perturbations

For simplicity and as suggested by experimental data, we consider in this section only the inviscid limit, and discuss successively the inhibition of cell division (Sec. 5.1), of actin polymerization (Sec. 5.2), and of contractility (Sec. 5.3). In each case, Eq. (19) allows in principle to predict the response of the front velocity to pharmacological perturbations with drugs known to affect the cell cycle, the actomyosin cytoskeleton and/or to interfere with cell motility.

5.1 Blocking cell proliferation

When $k_{\mathrm{d}} = 0$, the cell number density becomes a conserved quantity and the dimensional problem reads

$$\partial_t \rho - \frac{E}{\xi} \partial_{xx} \rho = 0,$$

$$\rho(L(t),t) = \rho_{\mathrm{e}} \, e^{-\frac{\sigma_{\mathrm{p}}}{E}}, \quad \partial_x \rho(0,t) = 0,$$

$$\dot{L} = -\frac{E}{\xi \rho_{\mathrm{e}}} \, e^{\frac{\sigma_{\mathrm{p}}}{E}} \, \partial_x \rho(L(t),t).$$

with an initial density profile $\rho(x, t = 0) = \rho^0(x)$, $x \in [0, L_0]$. This is a classical Stefan problem for which (see Chap. 18 of[49]) the front will stop at the distance

$$L_{\mathrm{stop}} = e^{\frac{\sigma_{\mathrm{p}}}{E}} \int_0^{L^0} \frac{\rho^0(x)}{\rho_{\mathrm{e}}} \mathrm{d}x, \tag{20}$$

which as expected increases with σ_{p}. When cell division is blocked by mitomycin during the collective migration of epithelial cells along cylindrical rods[2], cells in the bulk stop moving, and monolayer expansion becomes confined to the front rows, where cells are stretched. In addition, collective cell migration has been observed to stop at a finite distance in the absence of cell division in a two-dimensional scratch wound healing assay (see[25], where a finite L_{stop} was predicted on the basis of a Lagrangian description). Both observations are in qualitative agreement with our model. However, whether the distance predicted by Eq. (20) is correct has not been tested quantitatively.

5.2 Inhibiting actin polymerization

Inhibitors of actin polymerization are expected to lower σ_{p}, and thus to lead to a lower front velocity through the decrease of α, assuming all other parameters to be unchanged. This was indeed observed experimentally on cylindrical wires of radius $10 \, \mu\mathrm{m}$ using the Rac inhibitor NSC23766[2].

5.3 Inhibiting contractility

Contractility may be taken into account explicitly in the model through an additive, constant active stress $\sigma_{\mathrm{A}} > 0$ in the constitutive equation: $\sigma = -E \log(\rho/\rho_{\mathrm{e}}) + \eta \partial_x v + \sigma_{\mathrm{A}}$. Up to the definition
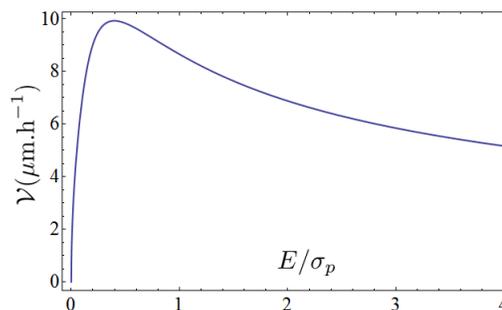
Fig. 5 Dimensional front velocity $\mathscr{V}$ **vs. effective elastic modulus** E/σ_{p}, for parameter values $\sigma_{\mathrm{h}} = 0$, $\tau_{\mathrm{d}} = 10^4 \, \mathrm{s}^{12}$, $\sigma_{\mathrm{p}} = 10^3$ Pa, $\sigma_{\mathrm{p}}/\xi = 0.1 \, \mu\mathrm{m}^2 \mathrm{s}^{-1 \, 4}$.

of a modified protrusive stress $\sigma_{\mathrm{p}} \to \tilde{\sigma}_{\mathrm{p}} = \sigma_{\mathrm{p}} - \sigma_{\mathrm{A}}$, the problem is unchanged. Again assuming all other parameters to be unaffected, inhibiting tissue contractility decreases σ_{A}, increases $\tilde{\sigma}_{\mathrm{p}}$, and therefore increases α. This simple argument suggests that inhibiting contractility would lead to a higher front velocity.

However, inhibitors of contractility may also modify tissue mechanics through indirect (or non-linear) effects on parameters other than σ_{A}. In[4], some among us conjectured that inhibiting the Rho pathway with C3-transferase may also increase the friction coefficient ξ, due to alterations of the density and turn-over of cell-substrate adhesions. Here, the same effect would lead to a lower front velocity according to Eq. (19).

Further, we expect contractility inhibition to decrease the tissue elastic modulus, as blebbistatin treatment is known to soften cells[50,51]. In Fig. 5, we plot the velocity $\mathscr{V}$ of the moving front as a function of E/σ_{p}, as obtained from Eq. (19), in the particular case $\rho_{\mathrm{d}} = \rho_{\mathrm{e}}$, i.e. $\sigma_{\mathrm{h}} = 0$. Strikingly, the curve $\mathscr{V}(E/\sigma_{\mathrm{p}})$ is not monotonic: a decrease of the tissue stiffness can result in either an increase or a decrease of the front velocity. Thus, the actual change of the front velocity may depend on the amplitude of the effect of contractility inhibition on the elastic modulus. Physically, this is due to the fact that in a softer material, growth generates less elastic stress pushing the free boundary but also resists less the pull generated by protrusive forces.

Together, we find that pharmacological inhibition of tissue contractility may therefore have an increasing or a decreasing effect on the front velocity depending on the concentration of the drug and on the respective amplitude of its impact on various physical parameters of the problem. Experimentally[1,2], blebbistatin treatment slows down the moving front in the case of narrow channels and fibers, whereas the effect is opposite for wider substrates.

Finally, let us emphasize that the possible effects of inhibitors have been inferred from known variations of the parameters σ_{p}, σ_{A}, ξ and E. To our knowledge, possible effects on the parameters τ_{d} and σ_{h} have not been studied and may modify our conclusions.

6 Conclusion

A simple description of a cell monolayer as a one-dimensional, proliferating, viscoelastic material allows to reproduce qualitatively a number of experimental observations pertaining to the

expansion of epithelial monolayers in a laterally confined geometry[1,2]: the displacement of the leading edge is linear in time; its velocity is of the order of $10\,\mu\text{m}\,\text{h}^{-1}$; the cell number density decreases while the velocity increases monotonically towards the moving front.

The active control parameter combines two mechanisms: protrusive forces generated by active crawling at the leading edge, and the mechanical effect of bulk cell proliferation. In the limit of small driving, an analytical solution predicts exponential relaxation of the density, velocity and stress profiles over a short boundary layer. In the limit of strong driving and zero viscosity, we recover the Fisher-Kolmogorov equation, a classical model of collective cell migration combining cell diffusion and proliferation. In this context, the diffusion coefficient receives a mechanical interpretation as the ratio of elastic modulus over tissue-substrate friction coefficient. In the case of strongly cohesive tissues, such as epithelial or endothelial monolayers, the cell density gradient is steep at the front. Indeed our description postulates a finite cell density at the free boundary, due to the presence of actively migrating leader cells. The Fisher-Kolmogorov approach predicts a smooth cell density gradient, and may thus better fit the expansion of high-density assemblies of mesenchymal cells, where cohesive forces are low and single cell diffusion contributes to the collective behavior.

Our one-dimensional model may also describe some aspects of the expansion of two-dimensional monolayers[52,53], provided that translational invariance in the direction orthogonal to front spreading is a reasonable approximation, in a statistical sense, thus allowing for averaging. Indeed similar one-dimensional models have been used to describe aspects of two-dimensional tissue expansion[6,7,25,26,46]. While a proper tensorial generalization remains highly desirable, this suggests that shear components may be neglected to first order when describing the mechanics of cell monolayers.

The model depends on two dimensionless parameters, the active driving α and the viscosity $\tilde{\eta}$. Although we provide an order of magnitude estimate for $\tilde{\eta} = 10^{-2}$, its relevance remains to be tested quantitatively since it builds on measurements performed on different geometries, sometimes with different cell types. Ideally, one would like to fit the model to experimental data, perhaps using velocity and cell density profiles to estimate model parameters. Given a linear relationship between proliferation rate and cell density, we used the framework of non-equilibrium linear thermodynamics and several simplifying, yet reasonable assumptions to predict that the tissue pressure should depend logarithmically on the cell density. This prediction may be tested experimentally, since the internal stress field can be obtained exactly in one spatial dimension from traction force microscopy[53]. As cell density increases in time, the same data may allow to estimate the critical value ρ_e where tissue pressure changes sign.

We deliberately selected the minimal set of mechanical ingredients conducive to a constant velocity of tissue expansion, and thereby neglected, among other ingredients, bulk cell motility, cell polarity, nonlinear tissue-substrate friction, or chemotaxis. It is our hope that appropriate modifications may make this work relevant to the modeling of *in vivo* collective cell migration[54], of which paradigmatic examples are the formation of the lateral line primordium[55,56], or neural crest cells migration[57].

A Evolution equation for arbitrary cell-division rate and elastic stress functions

The above results are obtained for a specific form of the net cell division rate $k_d(\rho)$, and an associated constitutive relation for the elastic stress that follows from non-equilibrium linear thermodynamics. For the sake of completeness, we give here the general evolution equations for the cell layer for arbitrary k_d and elastic stress $\sigma_e = -E s_e(\rho)$, with the sole constraints that they decrease monotonically with the density, $\mathrm{d}k_d/\mathrm{d}\rho < 0$, $\mathrm{d}\sigma_e/\mathrm{d}\rho < 0$, and vanish at finite values of the density. We show that once these functions are fixed, the evolution still depends on only two parameters, namely the active driving α and the effective viscosity $\tilde{\eta}$ identified above.

In the general case, the governing equations read

$$\partial_t \rho + \partial_x(\rho v) = k_d(\rho)\rho\,,$$

$$\partial_x \sigma = \xi v\,, \tag{21}$$

$$\sigma = -E s_e(\rho) + \eta\,\partial_x v\,,$$

respectively expressing cell number balance, force balance and the constitutive relation for the stress. They are supplemented with the boundary conditions

$$v(0) = 0\,, \qquad v(L) = \dot{L}\,, \qquad \sigma(L) = \sigma_p\,.$$

To simplify the notation in what follows, we introduce the following (by now familiar) conventions:

$$\rho_d \equiv k_d^{-1}(0)\,,$$

$$\rho_e \equiv s_e^{-1}(0)\,,$$

$$\sigma_h \equiv -E s_e(\rho_d)\,.$$

We furthermore define two auxiliary functions for the cell division rate and the elastic stress relative to the homeostatic density, or carrying capacity, of the tissue:

$$\kappa(x) \equiv k_d(x\rho_d)\,,$$

$$\bar{s}_e(x) \equiv s_e(x\rho_d) - s_e(\rho_d)\,.$$

Non-dimensionalizing with the units

$$t^* = 1\Big/\lim_{x\to 0}\kappa(x)\,, \quad l^* = \sqrt{E t^*/\xi}\,, \quad \rho^* = \rho_d$$

for time, length, and cell number density, respectively, and using

the previously introduced reduced stress

$$s = \frac{\sigma - \sigma_p}{E},$$

we can then recast Eqs. (21) in the simpler form

$$\frac{\partial \rho}{\partial t} + \frac{\partial}{\partial x}\left(\rho \frac{\partial}{\partial x}s\right) = \bar{k}_d(\rho)\rho,$$

$$\tilde{\eta}\frac{\partial^2 s}{\partial x^2} - s = \bar{s}_e(\rho) + \alpha,$$

(22)

where $\bar{k}_d(\rho) = \kappa(\rho)/\lim_{x\to 0}\kappa(x)$. The boundary conditions correspondingly become

$$\partial_x s(0) = 0, \qquad \partial_x s(L) = \dot{L}, \qquad s(L) = 0.$$

As in the specific case discussed in the main manuscript, for any given functions k_d and f the dynamics depends only on two dimensionless parameters given by

$$\alpha = \frac{\sigma_p - \sigma_h}{E}, \qquad \tilde{\eta} = \frac{\eta}{Et^*}.$$

Stationarity of (22) requires $\rho = 1$, $s = -\alpha$, and can only be attained for $\alpha = 0$ when taking the boundary condition on s into account.

We checked numerically that linear expansion is also observed for several plausible choices of the function $s_e(\rho)$ (see [27] for a proof in the inviscid limit). The curve $V(\alpha, \tilde{\eta})$ depends quantitatively on the precise form of the equation of state.

B Numerical resolution of the free boundary, viscous problem

B.1 Scaled variables

For the numerical resolution, in order to write boundary conditions at a fixed position in space, we prefer the scaled coordinate

$$y = \frac{x}{L(t)}.$$

(23)

and denote the new unknown functions $\hat{\sigma}(y,t) = \sigma[L(t)y,t]$ and $\hat{\rho}(y,t) = L(t)\rho[L(t)y,t]$. Eq. (1) becomes

$$\frac{\partial \hat{\rho}}{\partial t} + \frac{1}{L}\frac{\partial}{\partial y}(\hat{v}\hat{\rho}) = \hat{\rho}\left(1 - \frac{\hat{\rho}}{L}\right)$$

(24)

where the velocity field relative to the leading edge velocity can be expressed through the momentum conservation equation

$$\frac{1}{L}\frac{\partial \hat{s}}{\partial y} - y\dot{L} = \hat{v}$$

(25)

Using (25), the constitutive equation (11) becomes

$$\frac{\tilde{\eta}}{L^2}\frac{\partial^2 \hat{s}}{\partial y^2} - \hat{s} = \log(\frac{\hat{\rho}}{L}) + \alpha$$

(26)

Accordingly, the boundary conditions (12) become

$$\hat{v}(y=0,t) = 0$$

(27a)

$$\hat{v}(y=1,t) = 0$$

(27b)

$$\hat{s}(y=1,t) = 0$$

(27c)

B.2 Numerical implementation

The numerical scheme used to solve the Cauchy problem Eqs. (24-27) is based on the finite volume method [58] in order to strictly conserve mass and handle very localized states without spurious oscillations.

Two regularly-spaced grids on the same interval $[0,1]$, denoted Z and Z_d for its dual, are considered in parallel. An initial condition on $\hat{\rho}$ being given on Z, (26) is solved using boundary conditions (27a) and (27c) and the effective drift term $\hat{v}$ is computed on Z_d using relation (25). We then apply an upwind finite volume scheme to (24) using the no flux boundary conditions (27a) and (27b). This allows the computation of the updated concentration profile $\hat{\rho}$ on Z which gives in turn the new initial data used for the next time step. The same procedure is then repeated. The time interval for each time step is adapted so that the Courant-Friedrichs-Lewy condition is uniformly satisfied on Z_d [58].

References

1 S. R. K. Vedula, M. C. Leong, T. L. Lai, P. Hersen, A. J. Kabla, C. T. Lim and B. Ladoux, *Proc Natl Acad Sci U S A*, 2012, **109**, 12974–12979.

2 H. G. Yevick, G. Duclos, I. Bonnet and P. Silberzan, *Proc Natl Acad Sci U S A*, 2015, **112**, 5944–5949.

3 H. Yevick, *PhD thesis*, Université Pierre et Marie Curie, Paris, France, 2014.

4 O. Cochet-Escartin, J. Ranft, P. Silberzan and P. Marcq, *Biophys J*, 2014, **106**, 65–73.

5 J. D. Murray, *Mathematical Biology*, Springer, 2002.

6 P. K. Maini, D. L. S. McElwain and D. I. Leavesley, *Tissue Eng*, 2004, **10**, 475–482.

7 P. Maini, D. McElwain and D. Leavesley, *Appl. Math. Lett.*, 2004, **17**, 575–580.

8 S. Douezan and F. Brochard-Wyart, *Eur Phys J E*, 2012, **35**, 116.

9 H. Byrne and L. Preziosi, *Math Med Biol*, 2003, **20**, 341–366.

10 J. Ranft, J. Prost, F. Jülicher and J.-F. Joanny, *Eur Phys J E*, 2012, **35**, 9723.

11 M. BenAmar and M. Wu, *J R Soc Interface*, 2014, **11**, 20131038.

12 A. Puliafito, L. Hufnagel, P. Neveu, S. Streichan, A. Sigal, D. K. Fygenson and B. I. Shraiman, *Proc Natl Acad Sci U S A*, 2012, **109**, 739–744.

13 M. Basan, T. Risler, J.-F. Joanny, X. Sastre-Garau and J. Prost, *HFSP J*, 2009, **3**, 265–272.

14 J. Ranft, M. Basan, J. Elgeti, J.-F. Joanny, J. Prost and F. Jülicher, *Proc Natl Acad Sci U S A*, 2010, **107**, 20863–20868.

15 R. Farooqui and G. Fenteany, *J Cell Sci*, 2005, **118**, 51–63.

16 P. Chaikin and T. Lubensky, *Principles of Condensed Matter Physics*, Cambridge University Press, 2000.

17 P. Recho, J.-F. Joanny and L. Truskinovsky, *Phys. Rev. Lett.*, 2014, **112**, 218101.

18 C. Truesdell and W. Noll, *The non-linear field theories of mechanics*, Springer, 2004.

19 M. E. Gurtin, E. Fried and L. Anand, *The mechanics and thermodynamics of continua*, Cambridge University Press, 2010.

20 V. Berdichevsky, *Variational principles of continuum mechanics: I. Fundamentals*, Springer, 2009.

21 M. Epstein and G. A. Maugin, *Int J Plast*, 2000, **16**, 951–978.

22 J. Lowengrub and L. Truskinovsky, *Proc Roy Soc London A*, 1998, **454**, 2617–2654.

23 K. Garikipati, E. Arruda, K. Grosh, H. Narayanan and S. Calve, *J Mech Phys Solids*, 2004, **52**, 1595–1625.

24 D. Ambrosi, L. Preziosi and G. Vitale, *ZAMP*, 2010, **61**, 177–191.

25 Q. Mi, D. Swigon, B. Rivière, S. Cetin, Y. Vodovotz and D. J. Hackam, *Biophys J*, 2007, **93**, 3745–3752.

26 J. C. Arciero, Q. Mi, M. F. Branca, D. J. Hackam and D. Swigon, *Biophys J*, 2011, **100**, 535–543.

27 T. Stepien and D. Swigon, *SIAM J. Appl. Dyn. Syst.*, 2014, **13**, 1489–1516.

28 E. K. Rodriguez, A. Hoger and A. D. McCulloch, *J Biomech*, 1994, **27**, 455–467.

29 A. Goriely, M. Robertson-Tessi, M. Tabor and R. Vandiver, in *Mathematical Modeling of Biosystems*, Springer, 2008, ch. Elastic Growth Models, pp. 1–44.

30 M. H. Köpf and L. M. Pismen, *Soft Matter*, 2012, **9**, 3727–3734.

31 A. R. Harris, L. Peter, J. Bellis, B. Baum, A. J. Kabla and G. T. Charras, *Proc Natl Acad Sci U S A*, 2012, **109**, 16449–16454.

32 N. Podewitz, M. Delarue and J. Elgeti, *Europhys. Lett.*, 2015, **109**, 58005.

33 K. Guevorkian, M.-J. Colbert, M. Durth, S. Dufour and F. Brochard-Wyart, *Phys Rev Lett*, 2010, **104**, 218101.

34 T. V. Stirbat, A. Mgharbel, S. Bodennec, K. Ferri, H. C. Mertani, J.-P. Rieu and H. Delanoë-Ayari, *PLoS One*, 2013, **8**, e52554.

35 E. J. Doedel, *Cong. Numer.*, 1981, **30**, 255–384.

36 J. Ranft, M. Aliee, J. Prost, F. Jülicher and J.-F. Joanny, *New J Phys*, 2014, **16**, 035002.

37 X. Serra-Picamal, V. Conte, R. Vincent, E. Anon, D. T. Tambe,

E. Bazellieres, J. P. Butler, J. J. Fredberg and X. Trepat, *Nat. Phys.*, 2012, **8**, 628–634.

38 R. Fisher, *Ann. Eugenics*, 1937, **7**, 353–369.

39 A. Kolmogorov, I. Petrovsky and N. Piskunov, *Bull. Univ. État Mosc. (Bjul. Moskowskogo Gos. Univ.)*, 1937, **A1**, 1–26.

40 J. A. Sherratt and J. D. Murray, *Proc Biol Sci*, 1990, **241**, 29–36.

41 J. A. Sherratt and J. D. Murray, *Cell Transplant*, 1992, **1**, 365–371.

42 A. Q. Cai, K. A. Landman and B. D. Hughes, *J Theor Biol*, 2007, **245**, 576–594.

43 U. Savla, L. E. Olson and C. M. Waters, *J Appl Physiol*, 2004, **96**, 566–574.

44 B. G. Sengers, C. P. Please and R. O. C. Oreffo, *J R Soc Interface*, 2007, **4**, 1107–1117.

45 M. J. Simpson, B. J. Binder, P. Haridas, B. K. Wood, K. K. Treloar, D. L. S. McElwain and R. E. Baker, *Bull Math Biol*, 2013, **75**, 871–889.

46 A.-K. Marel, M. Zorn, C. Klingner, R. Wedlich-Söldner, E. Frey and J. O. Rädler, *Biophys J*, 2014, **107**, 1054–1064.

47 F. Sanchez-Garduno and P. Maini, *J. Diff. Eq.*, 1995, **117**, 281–319.

48 G. Bunting, Y. Du and K. Krakowski, *Networks Heterogen. Media*, 2012, **7**, 583–603.

49 J. Cannon, *The one-dimensional heat equation*, Addison-Wesley, 1984.

50 M. Balland, A. Richert and F. Gallet, *Eur. Biophys. J.*, 2005, **34**, 255–261.

51 J. C. Martens and M. Radmacher, *Pflugers Arch*, 2008, **456**, 95–100.

52 M. Poujade, E. Grasland-Mongrain, A. Hertzog, J. Jouanneau, P. Chavrier, B. Ladoux, A. Buguin and P. Silberzan, *Proc Natl Acad Sci U S A*, 2007, **104**, 15988–15993.

53 X. Trepat, M. R. Wasserman, T. E. Angelini, E. Millet, D. A. Weitz, J. P. Butler and J. J. Fredberg, *Nat. Phys.*, 2009, **5**, 426 – 430.

54 A. Aman and T. Piotrowski, *Dev Biol*, 2010, **341**, 20–33.

55 P. Haas and D. Gilmour, *Dev Cell*, 2006, **10**, 673–680.

56 S. J. Streichan, G. Valentin, D. Gilmour and L. Hufnagel, *Phys Biol*, 2011, **8**, 045004.

57 E. Theveneau and R. Mayor, *Dev Biol*, 2012, **366**, 34–54.

58 R. LeVeque, *Finite volume methods for hyperbolic problems*, Cambridge University Press, 2002.

Motivated by recent experiments on the expansion of highly cohesive cell sheets, our model of collective cell migration in one spatial dimension shows that constant front velocity results from the combined mechanical effects of bulk cell proliferation and front lamellipodial activity.